A Section 508–conformant HTML version of this article is available at https://doi.org/10.1289/EHP3730.

The Role of Peroxisome Proliferator–Activated Receptor Gamma (PPARγ) in Mono(2-ethylhexyl) Phthalate (MEHP)-Mediated Cytotrophoblast Differentiation

Hussein Shoaito,[1,2] Julia Petit,[2,3] Audrey Chissey,[1,2] Nicolas Auzeil,[2,3] Jean Guibourdenche,[1,2,4,5] Sophie Gil,[1,2,4] Olivier Laprévote,[2,3,6] Thierry Fournier,[1,2,4] and Séverine A. Degrelle[1,2,4,7]

[1]UMR-S1139, Faculté de Pharmacie de Paris, Institut national de la santé et de la recherché médicale (Inserm, National Institute of Health & Medical Research), Paris, France
[2]Université Paris Descartes, Sorbonne Paris Cité, Paris, France
[3]UMR 8638, Faculté de Pharmacie de Paris, Centre national de la recherche scientifique (Cnrs, National Center for Scientific Research), Paris, France
[4]Fondation PremUp, Paris, France
[5]Department of Biological Endocrinology, CHU Cochin, Assistance publique - Hôpitaux de Paris (AP-HP), Paris, France
[6]Department of Biochemistry, Hôpital Européen Georges Pompidou, AP-HP, Paris, France
[7]Inovarion, Paris, France

Background: Phthalates are environmental contaminants commonly used as plasticizers in polyvinyl chloride (PVC) products. Recently, exposure to phthalates has been associated with preterm birth, low birth weight, and pregnancy loss. There is limited information about the possible mechanisms linking maternal phthalate exposure and placental development, but one such mechanism may be mediated by peroxisome proliferator–activated receptor γ (PPARγ). PPARγ belongs to the nuclear receptor superfamily that regulates, in a ligand-dependent manner, the transcription of target genes. Studies of PPARγ-deficient mice have demonstrated its essential role in lipid metabolism and placental development. In the human placenta, PPARγ is expressed in the villous cytotrophoblast (VCT) and is activated during its differentiation into syncytiotrophoblast.

Objectives: The goal of this study was to investigate the action of mono(2-ethylhexyl) phthalate (MEHP) on PPARγ activity during *in vitro* differentiation of VCTs.

Methods: We combined immunofluorescence, PPARγ activity/hCG assays, western blotting, and lipidomics analyses to characterize the impacts of physiologically relevant concentrations of MEHP (0.1, 1, and 10 μM) on cultured VCTs isolated from human term placentas.

Results: Doses of 0.1 μM and 1 μM MEHP showed significantly lower PPARγ activity and less VCT differentiation in comparison with controls, whereas, surprisingly, a 10 μM dose had the opposite effect. MEHP exposure inhibited hCG production and significantly altered lipid composition. In addition, MEHP had significant effects on the mitogen-activated protein kinase (MAPK) pathway.

Conclusions: This study suggests that MEHP has a U-shaped dose–response effect on trophoblast differentiation that is mediated by the PPARγ pathway and acts as an endocrine disruptor in the human placenta. https://doi.org/10.1289/EHP3730

Introduction

Mono(2-ethylhexyl) phthalate (MEHP) is the primary metabolite of the common plasticizing agent di(2-ethylhexyl) phthalate (DEHP). DEHP is widely used in polyvinyl chloride (PVC) materials, which can easily accumulate in the body via exposure to medical devices, food, and indoor air (Chou and Wright 2006). Some phthalates have been shown to cross the placental barrier and have been detected in placental tissues, amniotic fluid, and cord blood (Mose et al. 2007). Indeed, an analysis of umbilical cord blood samples obtained from 84 consecutive newborns born in a single hospital in Italy detected a mean MEHP concentration of 0.52 ± 0.61 μg/mL [1.86 μM] (Latini et al. 2003). However, this concentration was dramatically higher in 21 maternal and 30 umbilical cord blood samples collected randomly from low birth weight (LBW) infants born in a third-grade Maternal and Child Health Hospital in Shanghai, China, (11.87 μg/ml [42 μM] and 9.94 μg/ml [35 μM], respectively; Lin et al. 2008). Furthermore, although published results have been inconsistent (Vrijheid et al. 2016), several studies have reported that maternal exposure to phthalates during pregnancy is linked to changes in placental size and shape (Zhu et al. 2017), fetal growth parameters (Huang et al. 2014; Song et al. 2018), preterm birth (Ferguson et al. 2014), pregnancy loss (Gao et al. 2017b), and altered neurodevelopment in infants (Engel et al. 2009) and children (Téllez-Rojo et al. 2013). In addition, phthalates are classified as endocrine-disrupting compounds as they adversely affect the endocrine system (Lyche et al. 2009).

Healthy fetal development is highly dependent on proper placental growth throughout pregnancy (Aplin and Jones 2008). During the process of placenta formation, mononucleated villous cytotrophoblasts (VCTs) either: *a*) proliferate and differentiate into highly invasive extravillous cytotrophoblasts (EVCTs), which can invade the maternal endometrium and remodel the spiral arteries, or *b*) fuse and form the continuous, multinucleated syncytiotrophoblast (ST). The ST, which forms the outermost surface of the placental chorionic villi, is located at the interface between maternal and fetal circulation. This multinucleated layer regulates gas and nutrient exchange, supports intensive endocrine functions, and provides immunological support to the fetus. A better understanding of the processes of differentiation and fusion of VCTs to form the ST is essential because disturbance of this regulation is thought to be associated with pregnancy disorders such as preeclampsia (PE) and intrauterine growth retardation (IUGR) (Huppertz and Kingdom 2004; Longtine et al. 2012; Roland et al. 2016). Fortunately, this fusion process can be studied *in vitro*, using primary cultures of VCT. The functionality of the ST is then assessed through the measurement of hCG released in the supernatant (Cocquebert et al. 2012; Tarrade et al. 2001).

Peroxisome proliferator–activated receptor γ (PPARγ) is a member of the nuclear receptor superfamily that binds the peroxisome proliferator response element (PPRE) sequence to regulate,

Address correspondence to Séverine A. Degrelle, INSERM, UMR-S1139, Faculté de Pharmacie de Paris, Paris F-75006, France. E-mail: severine.degrelle@inserm.fr or severine.degrelle@inovarion.com

Supplemental Material is available online (https://doi.org/10.1289/EHP3730).
The authors declare they have no actual or potential competing financial interests.
Received 4 April 2018; Revised 3 February 2019; Accepted 11 February 2019; Published 27 February 2019.

in a ligand-dependent manner, the transcription of target genes. PPARγ is involved in embryonic development (Barak et al. 1999; Nadra et al. 2010), lipid metabolism (Latruffe and Vamecq 1997; Schoonjans et al. 1996), insulin resistance (Giannini et al. 2004), inflammation (Giannini et al. 2004), immune response, and differentiation of several tissues, including the placenta and trophoblast (Barak et al. 1999; Tarrade et al. 2001). In the human placenta, PPARγ is expressed in *a*) EVCTs, as an essential regulator of EVCT invasion (Fournier et al. 2008) and *b*) VCTs, where its activation has been demonstrated during syncytialization (Schaiff et al. 2000; Tarrade et al. 2001). Furthermore, altered expression or activation of PPARγ has been observed in placental pathologies such as IUGR and PE (higher PPARγ expression (Holdsworth-Carson et al. 2010) and lower PPARγ activity (McCarthy et al. 2011; Waite et al. 2005), respectively).

Recent *in vitro* studies have reported that MEHP inhibits human EVCT invasion (Gao et al. 2017a) and hCG secretion by the villous trophoblast (Adibi et al. 2017b). These effects could potentially be mediated by MEHP acting as an exogenous ligand for PPARγ. For this reason, the possible role of PPARγ in the effects of MEHP on placental development and, more precisely, on VCT differentiation is of particular interest. The present study was designed to *a*) investigate the action of MEHP on *in vitro* differentiation of VCT and hCG secretion, *b*) characterize the effect of MEHP on PPARγ expression and activity, and *c*) analyze the lipid profiles of MEHP-treated cells.

Materials and Methods

Reagents

MEHP (#ALR-138N) was purchased from AccuStandard Inc., PPARγ agonist (GW1929, #ab142213) and antagonist (GW9662, #ab141125) from Abcam, and dimethyl sulfoxide (DMSO, #D2650) from Sigma-Aldrich.

Ethical Statement

The study was performed according to the principles of the Declaration of Helsinki. Placentas were obtained with the patients' written informed consent. The protocol was approved by the local ethics committee (CPP 2015-mai-13,909). Placental tissues were obtained from women who underwent normal cesarean section at the Cochin Port-Royal, Antony, and Montsouris maternity units (Paris, France). The reasons for cesarean section were as follows: breech delivery or transverse presentation, multiple scars on the uterus, and narrow pelvis. The women had otherwise uncomplicated pregnancies as determined from their medical health records. Because placentas are given anonymously, no details about the demographics of the population (age, race/ethnicity) or reason for the normal cesarean section could be obtained.

Distribution of Placental Materials

In this study, a total of $n = 23$ placentas (10 males and 13 females) were examined, with the number of placentas varying among experiments. For investigations of VCT viability/cytotoxicity/apoptosis, $n = 5$ placentas were used; for cell fusion/PPARγ activity assays and western blots, $n = 3$ placentas. For lipidomics analyses, which required a high number of treated cells and a high number of placentas to be significant, three treatments (vehicle, 0.1, and 10 μM MEHP) were performed on $n = 12$ placentas (5 males and 7 females). For hCG quantification in treated cells (vehicle, PPARγ agonist/antagonist, 0.1, 1 and 10 μM MEHP) $n = 11$ placentas (5 males and 6 females) were used; these corresponded to those used in the cell fusion/PPARγ activity assays ($n = 3$), western blots ($n = 3$), and some of those used in lipidomics analyses ($n = 5$) to ensure the donor-independency of the results.

Cell Culture and Treatment

VCTs were isolated from human term placentas ($n = 23$, 10 males and 13 females) as previously described (Alsat et al. 1991; Degrelle et al. 2017a; Frendo et al. 2003). Briefly, several cubic millimeters of the basal plate surface were removed with a sharp blade. Villous tissue was gently scraped free from blood vessels and connective tissue using forceps. After washing thoroughly two times with DMEM and once in 1X Ca^{2+}- and Mg^{2+}-free HBSS, the tissue was cut into small pieces. About 15 g of minced tissues were digested once in 50 ml of a filtered digestion enzyme medium, which contained 500 mg of trypsin powder (#27250-018, Sigma-Aldrich), 17.5 ml fat-free milk, 250 μl DNase I (50 U/ml), 250 μl 0.1 M $MgSO_4$ (#5886-0500, Merck) and 250 μl 0.1 M $CaCl_2$ (#1-02820-1000, Merck) in 250 ml warm 1X Ca^{2+}- and Mg^{2+}-free HBSS. The mixture was placed in a shaking incubator (50 rpm) at 37°C for 30 min. Then the tissues were incubated with 30 ml of the digestion medium for 10 min; this step was performed up to five times. Enzymatic degradation was monitored under light microscopy and was stopped by filtering the mixture through a 40-μm strainer into 50-ml tubes containing 5% FBS. Cell suspensions were collected and centrifuged at 1200 rpm for 10 min at room temperature. Cell pellets were suspended in 3 ml of DMEM, laid on top of a preformed Percoll gradient (60%, 50%, 45%, 35%, 30%, 20%, and 10%) and centrifuged at 2500 rpm at room temperature without braking for 20 min. The layer between 45% and 35% Percoll contained the trophoblast cells; this was collected, suspended in DMEM, and centrifuged at 1200 rpm at room temperature for 10 min. The resulting cell pellet was suspended in DMEM supplemented with 10% FCS, 2 mM glutamine, 100 IU/mL penicillin, and 100 μg/mL streptomycin (Gibco 15140-122), and the cells were counted using a TC20™ Automated Cell Counter (Biorad). The cells were cultured in 5% CO_2 at 37°C. After overnight incubation, cells were treated with MEHP, PPARγ agonist (1 μM GW1929), or PPARγ antagonist (1 μM GW9662). After 72 h of culture, cells were preserved in one of two ways: 1) fixed with 4% PFA for 20 min at room temperature, washed three times in PBS, then stored in PBS at 4°C until immunostaining was performed, or 2) snap-frozen: cells were washed two times with cold PBS, scraped into 1 ml cold PBS and transferred into a 1.5 ml tube. After centrifugation (a 10 s pulse at 14,000 rpm), the PBS supernatants were discarded and the cell pellets were snap-frozen in liquid nitrogen and stored at −80°C until RT-qPCR, western blot, or lipidomics analyses were conducted. Cell supernatants were collected and stored at −20°C until determination of hCG concentration was carried out. For explants cultures, chorionic villi from term placentas ($n = 3$) were cultured in triplicate, placed in a 24-well plate using a folded pin and cultured in 2 ml of DMEM supplemented with 10% FCS, 2 mM glutamine, 100 IU/mL penicillin, and 100 μg/mL streptomycin with or without MEHP (0.1 μM, 1 μM or 10 μM). After 48 h of culture, explants were fixed with 4% PFA overnight at 4°C, then washed 3 times and stored in 1X PBS at 4°C until use.

Cell Viability, Cytotoxicity, and Apoptosis Assays

The effect of MEHP on cell viability, cytotoxicity, and apoptosis was measured using the ApoTox-Glo™ Triplex Assay (#G6321) from Promega, following the manufacturer's instructions. We plated 40,000 cells/well of a 96-well plate (#3904, Corning).

After 16 h of culture, cells were exposed to 0.1, 1, 10, 50, 100, and 500 μM MEHP for 24 h and 48 h. This assay detects a fluorogenic, cell-permanent peptide substrate (GF-AFC) for the determination of live-cell protease activity, and a cell-impermanent, fluorogenic peptide substrate (bis-AAF-R110) for the quantification of dead-cell protease activity; in this way, it is possible to quantify cell viability and cytotoxicity using two proportional, inversely correlated measures. The live- and dead-cell proteases produce different products, AFC and R110, respectively, which have different excitation and emission spectra, allowing them to be detected simultaneously.

A third aspect of the assay quantifies luciferase fluorescence to measure apoptosis. For this, we added luminogenic DEVD-peptide substrate for caspase-3/7 and Ultra-Glo recombinant Thermostable Luciferase to cells, which were provided in the kit. The presence of Caspase-Glo® 3/7 Reagent resulted in cell lysis, followed by caspase cleavage of the substrate and generation of a "glow-type" luminescent signal produced by luciferase. Fluorescence at 400Ex/505Em (viability) and 485Ex/520Em (cytotoxicity) and luminescence were measured using an EnSpire Multimode Plate Reader (Perkin Elmer). The percentage of cells was determined by comparing the luminescent signal of MEHP-treated cells to vehicle (DMSO treatment).

Transfection

After 16 h of culture, cells were treated for 2 h with 0.1, 1, or 10 μM MEHP, 1 μM GW1929, or 1 μM GW9662, which were diluted in a culture medium containing 1X glutamine and 10% FCS (without PS). Before transfections, cells were washed and then incubated with Opti-MEM I medium without serum (#11058021, Gibco; 200 μl/12-well removable chamber, #81201, Ibidi, or 500 μl/24-well plate, #3524, Corning). PPARγ activity assays were performed as previously described (Degrelle et al. 2017b). Briefly, for transient transfection with PPRE-H2B-eGFP, VCTs were plated in 12-well cell-culture–treated plastic slides (40,000 cells/well). For transient transfection with PPRE-pNL1.3 or pNL1.3 basic secreted luciferase reporter as control, VCTs were plated in 24-well plates (250,000 cells/well). In both conditions, cells were transfected using Lipofectamine® 3000 (Invitrogen) following the manufacturer's protocol. Four hours later, the transfected cells were washed and treated again with 0.1, 1, or 10 μM MEHP, 1 μM GW1929, or 1 μM GW9662 for 48 h.

Immunofluorescence and Image Analysis

After 72 h of culture, cells were fixed in 4% PFA for 20 min at room temperature, washed in PBS, and permeabilized in 0.5% Triton X-100 in PBS for 30 min. Then, cells were blocked in 5% IgG-free BSA and placed in 0.1% Tween-20 in PBS for 1 h at room temperature. For the fusion index assay, cells were incubated overnight at 4°C with 2μg/ml of TWIST1 (#ab50887, Abcam) or GATA3 (#sc-268, Santa Cruz Biotechnology) and desmoplakin (#ab71690, Abcam) primary antibodies in blocking solution, as described in Degrelle and Fournier 2018. The next day, cells were rinsed three times with 0.1% Tween-20 in PBS (PBST), then the staining was revealed with the VectaFluor™ Excel R.T.U. Antibody Kit using DyLight® 488 Anti-Mouse IgG antibody (#DK-2488, Vector Laboratories) according to the manufacturer's instructions. After three washes with PBST, cells were incubated with Alexa Fluor® 555 Donkey anti-Rabbit IgG (H + L) Highly Cross-Adsorbed secondary antibody (#A31572, Invitrogen; 1:500 in PBST) for 1 h in the dark at room temperature, then washed three times in PBST and counterstained with DAPI for 10 min at room temperature. For PPRE-H2B-eGFP experiments, cells were incubated with Alexa Fluor® 555 Phalloidin (#A34055, Invitrogen; 1:200 in PBST) for 1 h, in the dark at room temperature, then washed three times in PBST, and counterstained with DAPI for 10 min at room temperature, as described in Degrelle et al. 2017b. Finally, slides were mounted with Fluoromount-G (#FP-483331, Interchim) and stored at 4°C. Confocal microscopy images (obtained with a Leica spinning-disk microscope equipped with a Plan Apo 63X/1.4 oil objective and a CoolSnap HQ2 CCD camera) were processed with ImageJ (National Institutes of Health; https://imagej.nih.gov/ij/) or Icy (Institut Pasteur; http://icy.bioimageanalysis.org/). The fusion index was calculated in three placentas from seven nonoverlapping images per replicate and determined as [% (number of TWIST1 + nuclei/total number of DAPI nuclei)] or [100 − % (number of GATA3 + nuclei/total number of DAPI nuclei)] as previously described (Degrelle and Fournier 2018). Quantification of PPRE-H2B-eGFP was performed on a minimum of 100 nuclei per condition in three independent experiments. For quantification, fluorescent signals were integrated over the entire nucleus as previously described (Degrelle et al. 2017b).

Neutral Lipid Staining

Placental explants were blocked in 5% IgG-free BSA in PBS for 1 h at room temperature and then incubated overnight at 4°C with BODIPY 505/515 (10μg/ml, Molecular probes) and Cytokeratin 7 (CK7, a trophoblast-specific marker) primary antibody (1 μg/ml, # SAB4501652, Sigma). The next day, explants were rinsed three times with PBS, and incubated 1 h at room temperature with an Alexa Fluor® 555 Donkey anti-Rabbit IgG (H + L) Highly Cross-Adsorbed secondary antibody (#A-31572, Invitrogen; 1:500 in PBS). After three washes with PBS, nuclei were counterstained with DAPI for 20 min at room temperature. Finally, slides were mounted with Fluoromount-G™ (#FP-483331, FluoProbes) and stored at 4°C. Confocal microscopy images were obtained with a Leica SP8 inverted microscope equipped with a Plan Apo oil-immersion x40 objective (numerical aperture 1.30). BODIPY fluorescence intensity ($n = 3$, 5 nonoverlapping images per replicate) was quantified with ImageJ (National Institutes of Health; https://imagej.nih.gov/ij/).

hCG Assay

hCG concentrations ($n = 11$, 5 males and 6 females) were measured using the CG + β assay on a cobas e801 analyzer (Roche). This immunoassay uses two different antibodies: a biotinylated monoclonal mouse antibody for capture and a monoclonal mouse antibody labeled with ruthenium for electrochemiluminescence detection (ECLIA). The parameters of the assay were as follows: range 1–10,000 UI/L, LOQ < 0.6 UI/L, no cross-reaction with FSH, TSH; LH = 0.12%, accuracy: within run CV < 3% and between run <8%.

RNA Isolation and Real-Time qPCR

Total RNA from cells was purified on RNeasy columns (Qiagen) according to the manufacturer's protocol and quantified using a Nanodrop spectrophotometer. Reverse transcriptions (250 ng total RNA) were performed using Superscript III (Invitrogen) with random hexamers. cDNA was prepared in duplicate and pooled to perform qPCR. As previously described (Segond et al. 2013), real-time quantitative RT-PCR was performed in triplicate with qPCR MasterMix Plus for SYBR Green (Eurogentec). using an ABI Prism 7900 Sequence Detection system (Applied Biosystems) under the following conditions: an initial denaturation step (95°C for 10 min); 40 cycles of 95°C for 15 s, then 60°C for

60 s; followed by a three-step dissociation phase of 15 s at 95°C, 30 s at 60°C, and 15 s at 95°C to eliminate possible artifacts such as oligonucleotide dimers. The primer sequences were as follows: PPARγ (Peroxisome proliferator–activated receptor gamma) forward primer: 5′- AGTGGGGATGTCTCATAATGCC-3′, reverse primer: 5′- AGGTCAGCGGACTCTGGATTC-3′; 18S forward primer: 5′- TCCCCCAACTTCTTAGAGG-3′, reverse primer: 5′- CTTATGACCCGCACTTACTG-3′; HPRT1 (Hypoxanthine Phosphoribosyltransferase1) forward primer: 5′-GGCGTCGTGATTAGTGATG-3′, reverse primer: 5′- CAGAGGGCTACAATGTGATG-3′; RPLP0 (Ribosomal protein lateral stalk subunit P0) forward primer: 5′- AACATCTCCCCCTTCTCCT-3′, reverse primer: 5′- ACTCGTTTGTACCCGTTGAT-3′; SDHA (Succinate dehydrogenase complex flavoprotein subunit A) forward primer: 5′- CCACCACTGCATCAAATTCATG-3′, reverse primer: 5′- TGGGAACAAGAGGGCATCTG-3′. The relative RNA expression of each gene was normalized with the geometric mean of four endogenous controls (18S, HPRT, RPLP0, and SDHA) using qBasePlus 2 Software (Biogazelle).

Western Blotting

Total cell extracts were prepared from snap-frozen cell pellets using RIPA buffer [5 mM Tris-HCl (pH 7.6), 150 mM NaCl, 1% NP-40, 1% bodium desoxycholate, 0.1% SDS, containing freshly added protease inhibitors (#539131, Calbiochem), and phosphatase inhibitors (#524629, Calbiochem)], and then sonicated. For mitogen-activated protein kinase (MAPK) analyses, protein lysates were centrifuged at $14{,}000 \times g$ for 10 min at 4°C, and the supernatants were transferred to a new tube. Protein concentrations were determined using the Pierce™ Micro BCA™ Protein Assay Kit (#23235, Thermo Scientific). Equal amounts of proteins (50 µg or 20 µg) were separated on 4–15% SDS-PAGE mini-PROTEAN® TGX™ precast protein gel under reducing conditions (DTT) and transferred onto a 0.2-µm nitrocellulose membrane using a Trans-blot® Turbo™ Transfer System (Bio-Rad). For PPARG experiments, after blocking with 5% nonfat milk in TBST at room temperature for 1 h, membranes were incubated with primary antibodies in blocking solution at 4°C overnight. For MAPK experiments, after blocking with 3% BSA/TBST at 4°C overnight, membranes were incubated with primary antibodies in 1% BSA/TBST at room temperature for 3 h. The membranes were then washed three times with TBST at room temperature for 5 min and incubated with secondary antibodies at room temperature for 1 h. Finally, membranes were washed three times with TBST at room temperature for 5 min and scanned with an Odyssey® Imaging System (Li-Cor). The primary antibodies were: anti-PPARγ [0.5 µg/ml (1:400; sc-7,196, Santa Cruz Biotechnology)], anti-phospho- extracellular signal-regulated kinase (ERK) (p-ERK, 1:1,000; #4370, Cell Signaling), anti-total-ERK (t-ERK, 1:1,000; #4695, Cell Signaling), anti-phospho-P38 (p-P38, 1:1,000; #4511, Cell Signaling), anti-total-P38 (t-P38, 1:1,000; #8690, Cell Signaling), anti-phospho- c-Jun NH_2-terminal kinase (JNK) (p-JNK, 1:1,000; #9255, Cell Signaling), anti-total-JNK (t-JNK, 1:1,000; #9252, Cell Signaling), anti-β-actin (0.2 µg/ml (1:20,000; #A5441, Sigma-Aldrich), and anti-vinculin (0.1 µg/ml (1:10,000; #V9131, Sigma-Aldrich). The secondary antibodies were: Alexa Fluor® 680-conjugated donkey anti-Mouse IgG (H + L) Highly Cross-Adsorbed (1:20,000; #A10038, Invitrogen) and Alexa Fluor® 790-conjugated donkey anti-Rabbit IgG (H + L) Highly Cross-Adsorbed (1:20,000; #A11374, Invitrogen). Signal intensity was quantified using ImageJ software (National Institutes of Health; https://imagej.nih.gov/ij/index.html). The arbitrary pixel densities of each protein were normalized to actin or vinculin.

Nanoluciferase Assay

VCTs transfected with PPRE-pNL1.3 or basic pNL1.3 were cultured in triplicate in a 24-well plate (see paragraph "Transfection"). After 24 h of treatment, 100 µl of each cell supernatant were dispensed into the wells of a 96-well plate (#3610, Corning) and frozen at −20°C. After 48 h of treatment, the frozen 96-well plate was heated to room temperature and 100 µl of each cell supernatant were dispensed into the wells of the same 96-well plate. The amount of secreted NanoLuc® luciferase activity was determined using the Nano-Glo® Luciferase Assay (#N1130, Promega) based on the manufacturer's instructions. Luminescence in each well was then measured using an EnSpire Multimode plate reader (Perkin Elmer). Each luminescence reading was normalized to the average of the corresponding not-transfected control cells.

Lipid Extraction and Liquid Chromatography Mass Spectrometry Analysis

Cell pellets from cells treated for 48 h with vehicle, 0.1 µM, or 10 µM MEHP (stored at −80°C after snap-freezing in liquid nitrogen; $n = 12$, 5 males and 7 females) were ground twice using a Precellys® 24-Dual grinder (Bertin Technologies) at 5,000 rpm with 1 mL water for 15 s. After homogenization, lipids were extracted twice with a mixture of *tert*-butyl methyl ether/methanol/water (10:3:2.5, v/v/v), which contained 0.01% (w/v) of 3,5 Di-tert-4-butylhydroxytoluene. After centrifugation at 3,000 rpm for 10 min, the supernatants were collected and evaporated under reduced pressure at 45°C. For the UPLC-MS analyses, lipid extracts were resuspended in an acetonitrile/isopropanol/chloroform/water mixture (35:35:20:10, v/v/v/v). Liquid chromatography-electrospray ionization mass spectrometry analysis of lipid extracts was performed on a Synapt® G2 High Definition MS™ (Q-TOF) mass spectrometer (Waters) combined with a UPLC system (Waters). Chromatographic separation was performed on an Acquity CSH C18 column (100×2.1 mm; 1.7 µm) set at 50°C; the binary gradient system used 10 mM ammonium acetate in an acetonitrile/water mixture as solvent A (40:60, v/v) and 10 mM ammonium acetate in an acetonitrile/isopropanol mixture as solvent B (10:90, v/v). The following gradient was applied: The run began with 40% of solvent B, ramped to 100% over 10 min, and was held for 2 min before a rapid return to initial conditions, followed by 2.5 min of equilibration. The flow rate was kept at 0.4 mL/min for 15 min. Data were collected both in positive (ESI +) and negative (ESI −) ionization modes at 50–1200 m/z in the full scan mode. The source parameters were as follows: capillary voltage 3,000 V (ESI +) and 2,400 V (ESI −), cone voltage 30 V (ESI +) and 45 V (ESI −), source temperature 120°C, desolvation temperature 550°C, cone gas flow 20 L/h, and desolvation gas flow 1,000 L/h. Leucine enkephalin was used as the external reference compound (Lock-Spray™) for mass correction at a concentration of 0.2 ng/mL. Data were acquired in the resolution mode (20,000 FWHM at m/z 500) with a scan time of 0.1 s. Data acquisition was performed using Waters MassLynx™ software (version 4.1; Waters MS Technologies). XCMS was used for peak selection, deconvolution, alignment, and retention time correction, and to generate peak tables of m/z and retention time pairs with associated relative intensities for all detected peaks. Data were median centered, $\log_{10}$ transformed, and Pareto scaled before multivariate analyses.

Statistical Analyses

For cell viability, cytotoxicity, and apoptosis assays; nanoluciferase assays; western blots; quantification of fusion index; hCG secretion; and immunofluorescence imaging (PPRE-H2B-eGFP),

all measurements were performed with at least three independent placentas. The data are expressed as the mean ± SEM of the indicated number for cell viability, cytotoxicity, apoptosis, and nanoluciferase assays, or mean + SD of the indicated number for western blots and experiments on the fusion index, hCG secretion, and PPRE-H2B-eGFP. Statistical analysis (paired *t*-test) of each treated group vs. vehicle control was performed using GraphPad Prism 6.07 software. Results were considered significant if the *p*-value was <0.05 (*), <0.01 (**), <0.001 (***) or <0.0001 (****). For lipidomics experiments, multivariate statistical analyses were performed with SIMCA-P+ software 13.0.3 (Umetrics). Models were constructed using an unsupervised principal component analysis (PCA), a supervised partial least squares-discriminant analysis (PLS-DA), or orthogonal projections to latent structures-discriminant analysis (OPLS-DA). Variables were selected as potential markers according to their |p (corr)| (≥0.5) and Variable Importance in the Projection (VIP) score (>1) from the OPLS-DA analysis. Lipids were annotated by comparing the experimental data against lipid metabolite databases, including metlin (metlin.scripps.edu) and lipidmap (www.lipidmaps.org) with a tolerance of 5 ppm. Accuracy on retention time (tR) values was used to confirm annotation, with a threshold at 15%. A univariate data analysis (Wilcoxon) with a false discovery rate [(FDR)-adjusted $p < 0.01$] controlling the false-positive rate associated with multiple comparisons, was performed to assess the whole lipids identified and the statistical significance of the difference in concentration in MEHP-treated (0.1 or 10 μm) lipid extracts between compared control (vehicle) samples.

Results

Effect of MEHP on Cell Viability, Cytotoxicity, and Apoptosis in Human Primary Cytotrophoblasts

To evaluate the effect of MEHP on cell viability, cytotoxicity, and apoptosis, human primary cytotrophoblasts were exposed to MEHP at a serial dilution of 0.1 to 500 μm for 24 h or 48 h. In comparison with treatment with vehicle (DMSO), treatment with 50 μm or higher concentrations of MEHP resulted in significantly lower cell viability at 24 h and 48 h (Figure 1, left panel). Only treatment with 500 μm MEHP had a significant effect on cytotoxicity at 24 h and 48 h, as assessed by an extracellular protease activity assay for membrane integrity (Figure 1, middle panel). Furthermore, treatment with 50 μm or higher concentrations of MEHP resulted in significantly greater apoptosis [caspase 3/7 activity, Figure 1, right panel, or cleaved cytokeratin 18 (cCK18) immunostaining, Figure S1A] at 24 h and 48 h than did treatment with vehicle. We observed no differences in cell viability, cytotoxicity, or apoptosis with media alone in comparison with vehicle control at 24 h and 48 h (Figure S1B). Accordingly, we conducted the remainder of the experiments with nontoxic concentrations of MEHP: 0.1, 1, and 10 μM. These concentrations are also consistent with those used on mouse 3T3-L1 (Manteiga and Lee 2017) and on chicken germ cells (Guibert et al. 2013).

Effect of MEHP on Human VCT Differentiation

To investigate the effect of MEHP on the *in vitro* differentiation of human cytotrophoblast into STs, index fusion was calculated based on TWIST1 (Figure 2A,B) or GATA3 (Figure S2A,B) immunostaining. In comparison with vehicle control, treatment with 10 μM MEHP showed a significantly higher level of syncytialization (70% vs. 55%; $p < 0.0001$), similar to that obtained after treatment with the PPARγ agonist (1 μM GW1929; 75%). Instead, treatments with 0.1 or 1 μM MEHP showed a significantly lower level of syncytialization (33%, 32%, respectively vs. 55%; $p < 0.0001$), similar to treatment with the PPARγ antagonist (1 μM GW9662; 32%).

Effect of MEHP on hCG Secretion

Levels of hCG released by cytotrophoblasts in culture media were analyzed in the same cultures depicted in Figure 2A,B and Figure S2A,B. It is interesting to note that cytotrophoblasts exposed to MEHP, regardless of MEHP concentration (Figure 2C) or the sex of the cells (Figure S2C), released significantly less hCGβ (30–40% of control; $p < 0.0001$). These results support the idea that MEHP exposure inhibits hormonal functions in the cytotrophoblast.

Effect of MEHP on PPARγ Expression and Transcriptional Activity during Human VCT Differentiation

To investigate the involvement of PPARγ in the responses elicited by MEHP, we first looked at the mRNA and protein expression of PPARγ. qPCR analysis revealed that in comparison with vehicle control, treatment with 10 μM MEHP resulted in significantly higher PPARγ mRNA expression ($p < 0.001$), whereas treatments with 0.1 μM yielded significantly lower PPARγ mRNA expression ($p < 0.01$). However, western blot analysis showed that MEHP exposure did not alter the levels of PPARγ proteins (Figure S3). We thus assessed the effect of MEHP on

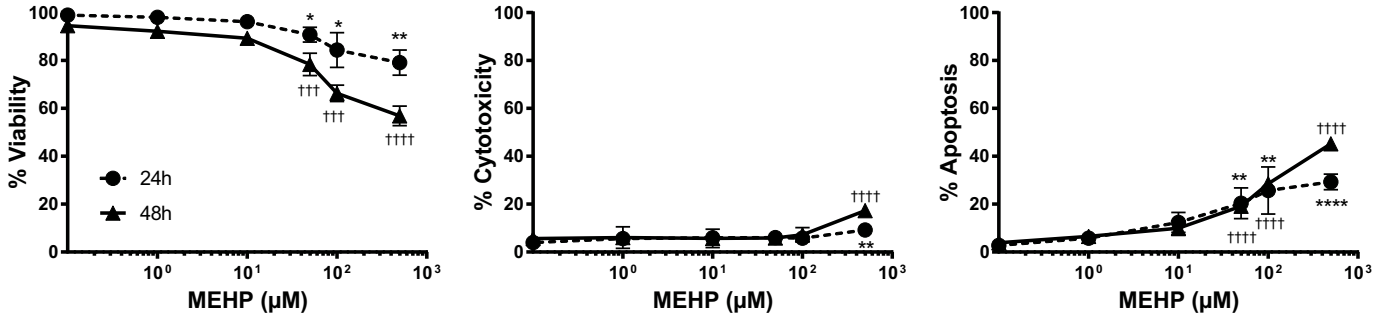

Figure 1. Effect of MEHP on VCT viability, cytotoxicity, and apoptosis as determined by ApoTox-Glo Triplex Assay (Promega). Cells were treated with various concentrations of MEHP (0.1, 1, 10, 50, 100, or 500 μM) for 24 h (circle, dashed line) or 48 h (triangle, solid line). The percentages were determined by comparing the fluorescent or luminescent signal of MEHP-treated cells to that of the vehicle (DMSO treatment). Values are presented as mean ± SEM. ($n = 5$, in triplicate). Note: DMSO, dimethylsulfoxide; MEHP, mono(2-ethylhexyl) phthalate; ST, syncytiotrophoblast; VCT, villous cytotrophoblast. Statistical analysis was performed using paired *t*-test in comparison with vehicle control; *, †$p < 0.05$, **, ††$p < 0.01$, ***, †††$p < 0.001$, ****, ††††$p < 0.0001$. The asterisk (*) indicates statistical significance of 24 h-treated cells, and the dagger (†) indicates statistical significance of 48 h-treated cells.

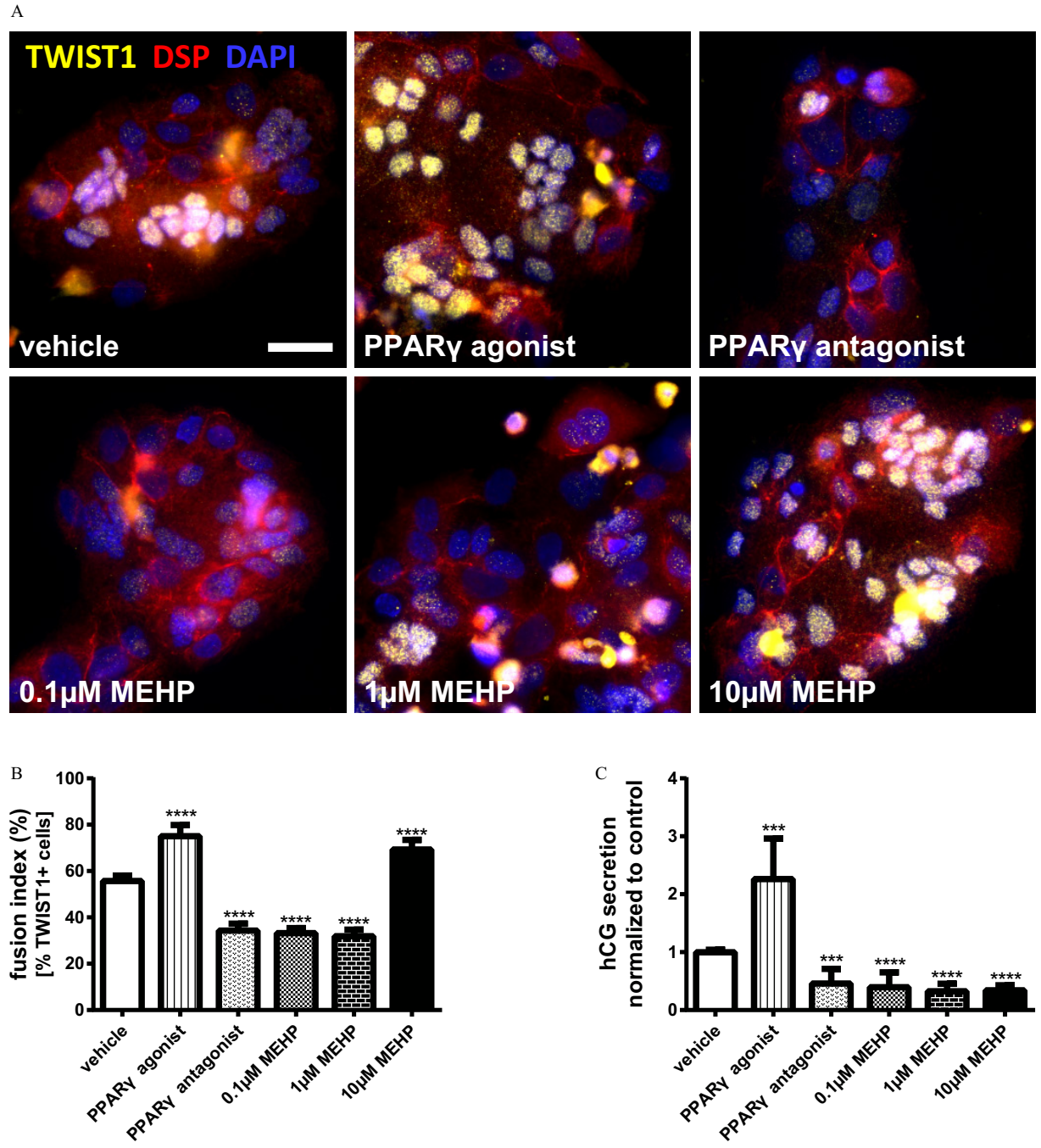

Figure 2. Effect of MEHP on trophoblast cell fusion and hCG secretion. After 16 h of culture, VCTs were treated for 48 h with either MEHP (0.1, 1, or 10 μM) or 1 μM of PPARγ agonist (GW1929) or antagonist (GW9662). After 72 h of culture, (*A*) representative images are shown of cells fixed and subjected to fusion assay [VCT and ST nuclei were immunostained with anti-TWIST1 (marker of ST, yellow) and anti-DESMOPLAKIN (red) antibodies and counterstained with DAPI (blue)]. Scale bar: 20 μm. (*B*) Nuclei were counted manually using the "cell counter" plugin of ImageJ. Fusion index (%) was calculated as the % (number of TWIST1 + nuclei/total number of nuclei). Values are represented as mean + SD of the percentage ($n = 3$ placentas, 7 non-overlapping images per replicate). (*C*) After 72 h of culture, hCG secretion was quantified in the media ($n = 11$). Values are presented as mean + SD of value normalized to vehicle control. Note: MEHP, mono(2-ethylhexyl) phthalate; PPARγ, peroxisome proliferator-activated receptor gamma; ST, syncytiotrophoblast; VCT, villous cytotrophoblast. Statistical analysis was performed using paired *t*-test in comparison with vehicle control; ***$p < 0.001$, ****$p < 0.0001$.

PPARγ transcriptional activity using two new reporter assays that we developed (Degrelle et al. 2017b). The transfection of cytotrophoblasts with PPRE-H2B-eGFP plasmid created eGFP + nuclei that reflected the intensity of PPARγ transcriptional activity (Figure 3A,B,D). In comparison with vehicle control, treatment with 10 μM MEHP resulted in significantly higher PPARγ activity (272 vs. 195; $p < 0.0001$), whereas treatments with 0.1 or 1 μM yielded significantly lower PPARγ activity (58 and 27, respectively, vs. 195; $p < 0.0001$). The transfection of cytotrophoblasts with the PPRE-pNL1.3[secNluc] plasmid confirmed this: There was significantly higher PPARγ activity with 10 μM MEHP (190 vs. 156; $p < 0.001$) and significantly lower PPARγ activity with 0.1 and 1 μM MEHP (126 and 100, respectively vs. 156; $p < 0.001$) after 48 h of treatment (Figure 3C–3E).

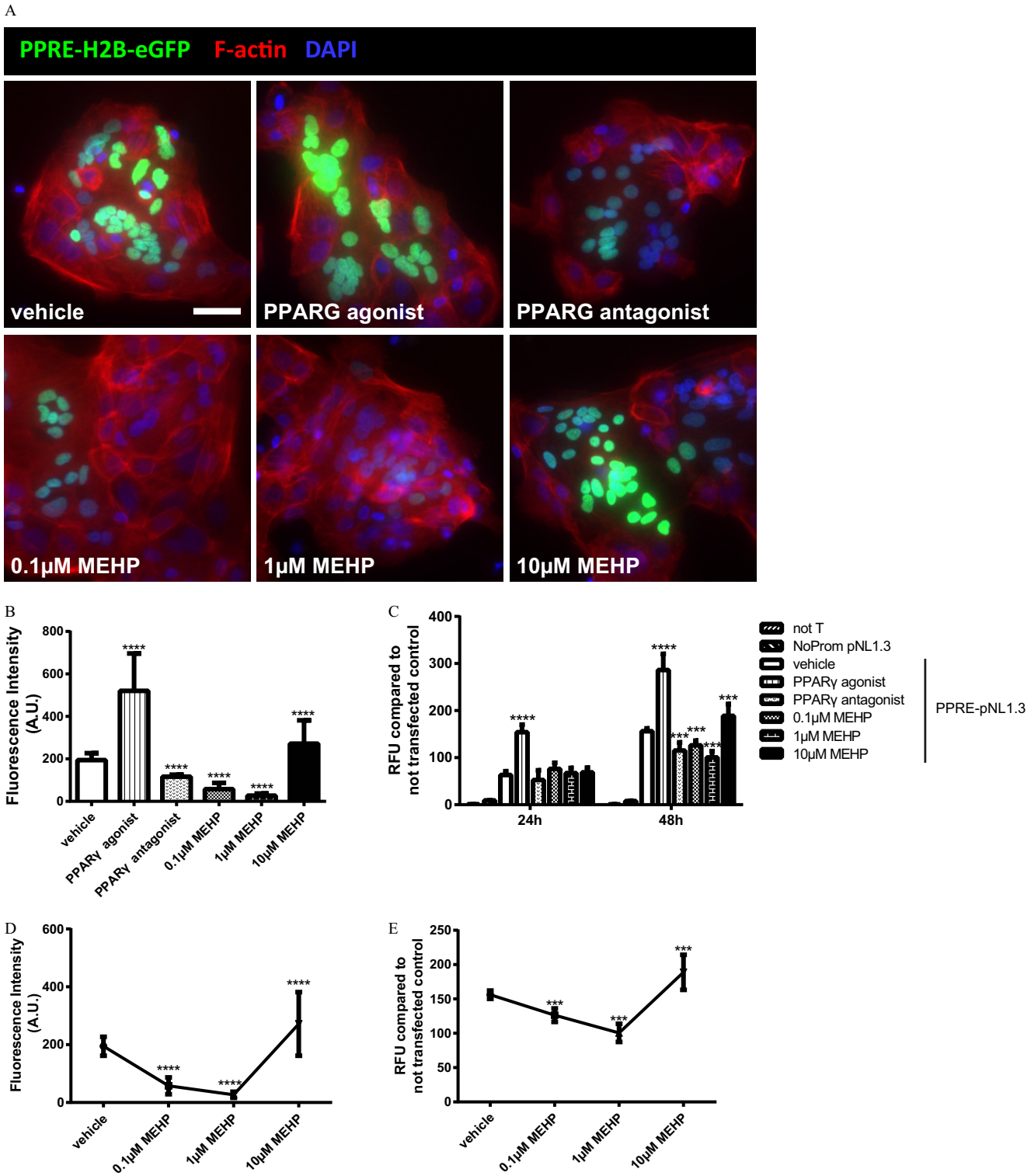

Figure 3. Effect of MEHP on PPARγ activity. After 16 h of culture, VCTs were pretreated for 2 h with MEHP (0.1, 1, or 10 µM) or 1 µM of PPARγ agonist (GW1929) or antagonist (GW9662). They were transfected for 4 h with PPRE-H2B-eGFP (green) or PPRE-pNL1.3[secNluc], then again received their original treatment for the next 48 h. PPARγ activity was first assayed by immunofluorescence: (*A*) cells were fixed, stained with phalloidin (red), and counterstained with DAPI (blue); then (*B*) PPRE-H2B-eGFP fluorescence intensity was quantified. Scale bar: 20 µm. We also determined PPARγ activity using the (*C*) Nano-Glo® Luciferase system (Promega). For each condition (triplicate), 100 µl of culture media after 24 h or 48 h of treatment were analyzed and compared with not-transfected cells. (*D–E*) Data from 2B (*D*) and 2C (*E*) represented as dose–response curves following 48 h of treatment with different concentrations of MEHP (0.1, 1, and 10 µM) and control (vehicle). Values are presented as mean ± SD of the fluorescence intensity (*B, D*) ($n = 3$, >100 nuclei) or mean ± SEM of the fluorescence intensity normalized to the not-transfected control (*C, E*) ($n = 3$ in triplicate). Note: MEHP, mono(2-ethylhexyl) phthalate; PPARγ, peroxisome proliferator-activated receptor gamma; ST, syncytiotrophoblast; VCT, villous cytotrophoblast. Statistical analysis was performed using paired *t*-test in comparison with vehicle control; ***$p < 0.001$, ****$p < 0.0001$.

Effect of MEHP on Lipid Profiles

To follow up on the observation that MEHP treatment significantly perturbed the activity of PPARγ, a key regulator of lipid metabolism, we performed BODIPY staining on placental explants treated with vehicle, 0.1 μM, or 10 μM MEHP. The appearance of the lipid vesicles is presented in Figure 4A, with the lipid vesicles stained green in the ST and mesenchymal cells (MC). In comparison with vehicle control, treatment with 10 μM MEHP resulted in significantly higher levels of lipid droplets (Figure 4B). Instead, treatments with 0.1 or 1 μM MEHP showed significantly lower levels of lipid droplets (Figure 4B). To compare the global lipid profiles of cytotrophoblasts that were treated with vehicle, 0.1, and 10 μM MEHP for 48 h, UPLC/QTOF MS data were used in PCA, PLS-DA, and OPLS-DA. OPLS-DA score plots showed a significant separation among the three groups (Figure 5A–E), in both positive mode (Figure 5A,C,D,E), and negative ion mode (Figure 5B). As shown in Table S1, treatment with 0.1 μM MEHP and 10 μM MEHP affected the expression of 50 and 115 lipid species, respectively. Among these were glycerophospholipids, including lysophosphatidic acids (LPA), lysophosphatidycholines (LPC), lysophosphatidylethanolamines (LPE), lysophosphatidylglycerols (LPG), phosphatidic acids (PA), phosphatidylcholines (PC), phosphatidylethanolamines (PE), phosphatidylglycerols (PG), and phosphatidylserines (PS), as well as glycerolipids such as diglyceride (DG), monoacylglycerols (MG), and fatty acids (FA). Analysis and quantification of individual classes of lipids from the total lipid fraction are shown in Figure 5F. In comparison with vehicle control, cells treated with 0.1 μM or 10 μM MEHP showed different lipid profiles. Overall, cells treated with 10 μM MEHP showed significantly higher levels of all glycerolipids (FA, MG, DG), PC, PS, phosphatidylserine plasmalogens (PS-P), and phosphatidic acid plasmalogens (PA-P) than cells treated with 0.1 μM MEHP or controls showed. The former group also showed significantly lower levels of phosphatidylcholine plasmalogens (PC-P) and phosphatidylethanolamine plasmalogens (PE-P) than the latter or controls showed. Instead, 0.1 μM MEHP-treated cells showed significantly lower levels of PC, LPG, PS, PS-P and all phosphatidic acid subclasses (PA, PA-P, LPA) than 10 μM MEHP-treated cells or controls showed. Regardless of the concentration (0.1 μM or 10 μM), MEHP-treated cells had significantly higher levels of LPE and PG.

Effect of MEHP on MAPK Pathway

We also examined the effects of MEHP on the MAPK pathway, which is essential for cytotrophoblast differentiation (Vaillancourt et al. 2009). After 72 h of culture, *in vitro* differentiated ST were treated with vehicle, 0.1, 1, or 10 μM MEHP for 15 and 30 min; we then determined differences in activation of ERK, P38, and JNK by western blotting (Figure 6A). In comparison with vehicle control, all MEHP-treated ST (except 15-min treatment with 1 μM MEHP) had significantly higher ratios of p-ERK/t-ERK and p-P38/t-P38; notably, we observed a U-shaped dose-dependent pattern activation of ERK and P38 (Figure 6B). In comparison with vehicle control, 15-min treatment with 1 μM or 10 μM MEHP resulted in a significantly lower ratio of p-JNK/t-JNK, whereas a 30-min treatment with 0.1 μM or 10 μM MEHP yielded a significantly higher ratio of p-JNK/t-JNK and a significantly lower ratio of p-JNK/t-JNK, respectively (Figure 6B).

Discussion

The majority of previous studies aimed at monitoring MEHP in pregnant women have focused on blood or urine samples (Adibi et al. 2008; Latini et al. 2003; Lin et al. 2008). *In vitro* studies offer the opportunity to characterize the responses of specific cell types to a chemically defined pollutant in isolation from systemic influences. Using this approach, our study demonstrated, to our knowledge for the first time, that MEHP affects villous trophoblast differentiation. Importantly, the doses employed in this study reflected physiologically relevant concentrations that have been detected in pregnant women [0.7 μM in maternal urine (Adibi et al. 2017a), 2.45 μM and 1.86–2.45 μM in maternal and cord blood, respectively (Latini et al. 2003), and 42 μM and 35 μM in maternal and cord blood, respectively, in cases of LBW infants (Lin et al. 2008)].

Previous studies on the effects of MEHP on PPARγ in the trophoblast have mostly used cell lines. For example, experiments in human HTR-8/SVneo cells showed that MEHP inhibits human extravillous trophoblast invasion via the PPARγ pathway (Gao et al. 2017a), and analysis of rat HRP-1 cells showed that MEHP disturbs the mRNA expression of PPARγ (Xu et al. 2005). In these studies, a relatively high dose of MEHP was used (100 μM and 50 μM, respectively). A more recent study performed on primary VCTs showed that after 40 h of treatment with 0.7 μM MEHP, hCG secretion decreased significantly in a sex-independent manner (Adibi et al. 2017b). The authors found no change in PPARγ protein expression, but no further investigation was done on PPARγ activity, lipid metabolism, and VCT differentiation. The results of our study were in concordance with these previous reports (no change in PPARγ protein expression, inhibition of hCGβ); however, to our knowledge, ours is the first study to report a U-shaped or nonmonotonic dose–response curve (NMDRC) for MEHP exposure on PPARγ activity.

The syncytialization of cytotrophoblast cells is central to human placental exchanges and hormone production (Huppertz and Gauster 2011). As syncytialization occurs, differentiated VCTs develop hormonal functions, with the increased synthesis and secretion of pregnancy hormones such as hCG. However, increased syncytialization without concomitant increases in hCG level has been previously observed in a study on the impact of formaldehyde on trophoblast differentiation and hormonal functions (Pidoux et al. 2015). As we observed here, those authors found that formaldehyde-exposed trophoblasts displayed an increase in cell fusion in comparison with control and showed a significant decrease in total hCG secretion. However, this study did not explain the molecular mechanism for the adverse effects on hCG secretion, but we know that changes in ST mass, formation, regeneration, or functioning can lead to abnormal endocrine production and provoke abnormal fetal development and miscarriage. Furthermore, hCG also acts in a paracrine and autocrine manner to trigger villous trophoblast differentiation and turnover throughout pregnancy (Pidoux et al. 2007). Clearly, the increased syncytialization we observed did not translate into improvement of trophoblast function, because we also observed a loss of secretion of hCG, the most important hormone of pregnancy. The production and secretion of hCG is essential at the beginning of pregnancy to induce progesterone synthesis by the ovarian corpus luteum, which leads to myometrium relaxation. In addition, through the first trimester of pregnancy, hCG is implicated in fusion and invasion processes of cytotrophoblasts and angiogenesis (Fournier et al. 2015). Our results suggest that MEHP exposure alters cytotrophoblast differentiation and will probably affect fecundity as well as time of pregnancy, even if a few studies have actually found higher levels of phthalates to be associated with shorter time to pregnancy or reduced risk of early pregnancy loss (Buck Louis et al. 2014; Jukic et al. 2016; Vélez et al. 2015).

Both low-dose effects and NMDRCs have been observed for a wide variety of endocrine-disrupting chemicals (EDCs) such as Bisphenol A (Vandenberg et al. 2012). EDCs accomplish this disruption by mimicking or blocking the action of endogenous

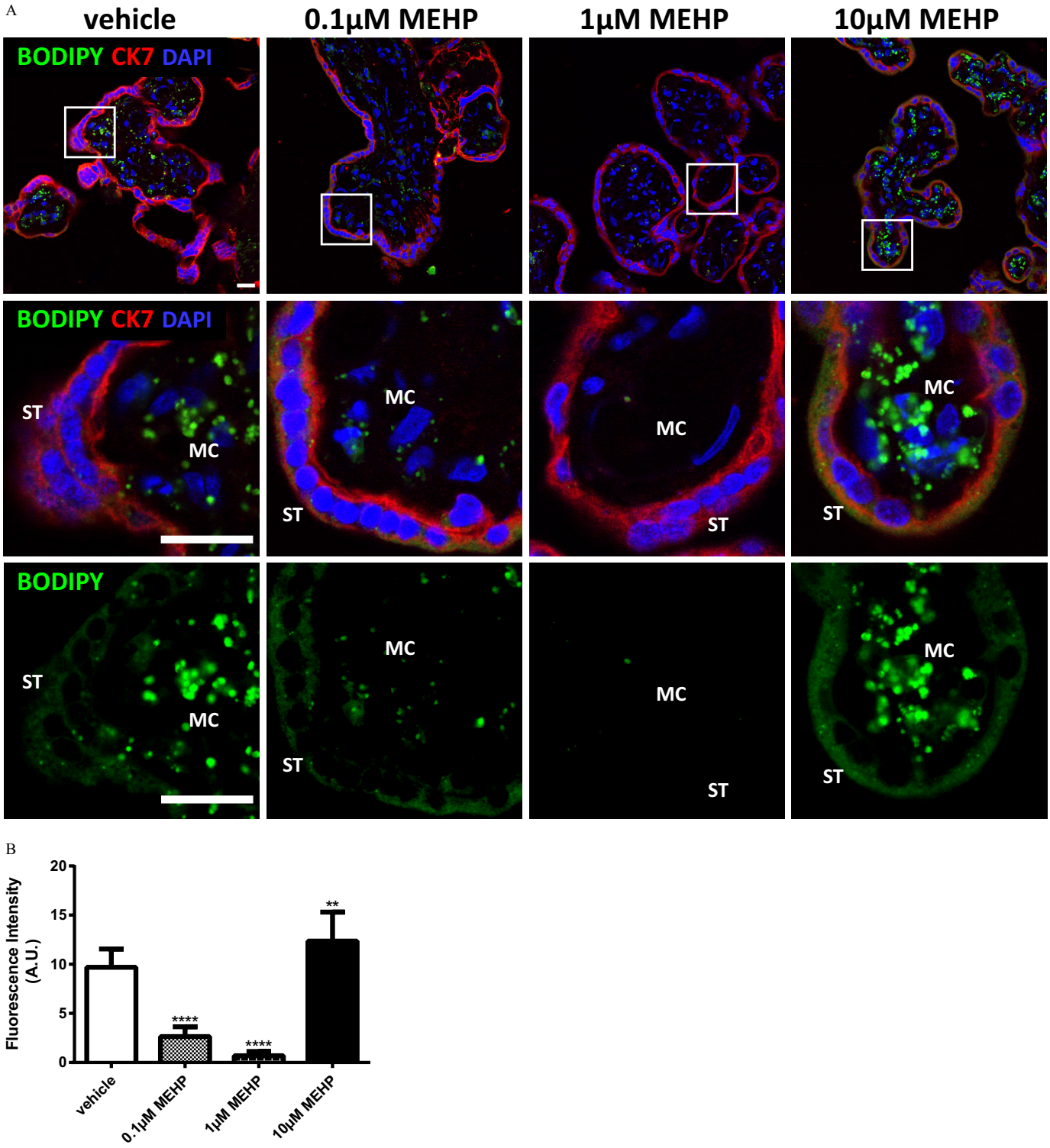

Figure 4. Effect of MEHP on lipid synthesis in human term placental explants. Placental explants were treated for 48 h with MEHP (0.1, 1, or 10 µM). (*A*) Representative images are shown of placental explants fixed and subjected to lipid droplet labeling. Placental explants were stained with BODIPY (505/515, green), immunostained with anti-cytokeratin 7 (CK7, red) antibody (a trophoblast-specific marker), and then counterstained with DAPI (blue). Scale bar: 20 µm. (*B*) Quantification of total fluorescence of BODIPY. Values are presented as mean + SD of the fluorescence intensity ($n = 3$, 5 non-overlapping images per replicate). Note: MC, mesenchymal cells; MEHP, mono(2-ethylhexyl) phthalate; ST, syncytiotrophoblast. Statistical analysis was performed using paired t-test compared to vehicle control; $^{**}p < 0.01$, $^{****}p < 0.0001$.

hormones, resulting in the inappropriate activation or inactivation of downstream pathways. Docking simulations to predict the binding mode of MEHP to the ligand-binding domain of PPARγ have shown 30 possible conformations and multiple interaction sites (Kambia et al. 2008). Furthermore, NMDRCs can occur because of differences in receptor affinity, and thus the response

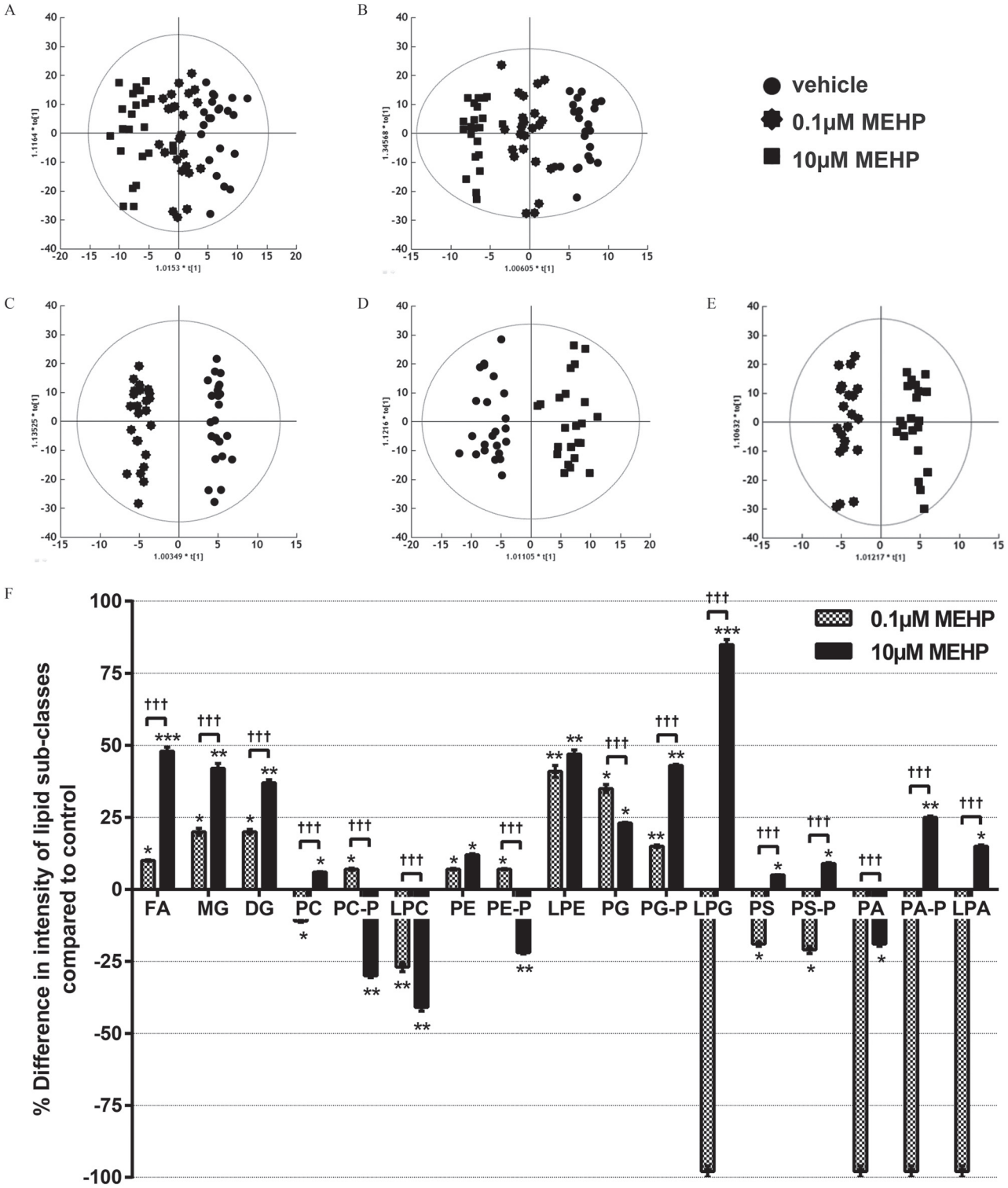

Figure 5. Effect of MEHP on lipid metabolic profiles. OPLS-DA score plots are shown of the cellular lipidome in cells that were treated with control (DMSO vehicle) or MEHP (0.1 μM or 10 μM) ($n = 12$ per group). Lipid profiles were obtained in (*A*) positive ionization mode and (*B*) negative ionization mode. (*C*) OPLS-DA score plots are shown of the cellular lipidome in positive ionization mode from cells treated with vehicle or 0.1 μM MEHP, (*D*) vehicle or 10 μM MEHP, or (*E*) 0.1 μM or 10 μM MEHP. (*F*) Intensities of lipid subclasses in vehicle- and MEHP-treated cells. The intensity of a subclass corresponds to the mean + SEM of the intensities of each lipid in all samples belonging to the same class. A univariate data analysis (Wilcoxon) corrected for the false discovery rate ((FDR)-adjusted $p < 0.01$) was performed between MEHP-treated (0.1 or 10 μM) cells in comparison with vehicle control; *$p < 0.05$, **$p < 0.01$, ***, †††$p < 0.001$. The asterisk (*) indicates a statistically significant difference between MEHP-treated cells (0.1 or 10 μM) and vehicle-treated cells, and the dagger (†) indicates statistical a significant difference between of 0.1 μM and 10 μM MEHP-treated cells. Details of lipid species that were differentially expressed among these lipid sub-classes are listed in Table S1. Note: DG, diacylglycerols; DMSO, dimethylsulfoxide; FA, fatty acids; LPA, lyso-PA; LPC, lyso-PC; LPG, lyso-PG; LPE, lyso-PE; MEHP, mono(2-ethylhexyl) phthalate; MG, monoacylglycerols; PA, phosphatidic acids; PA-P, PA plasmalogens;PC, phosphatidylcholines; PC-P, PC plasmalogens; PE, phosphatidylethanolamines; PE-P, PE plasmalogens; PG, phosphatidylglycerols; PG-P, PG plasmalogens; PS, phosphatidylserines; PS-P, PS plasmalogens.

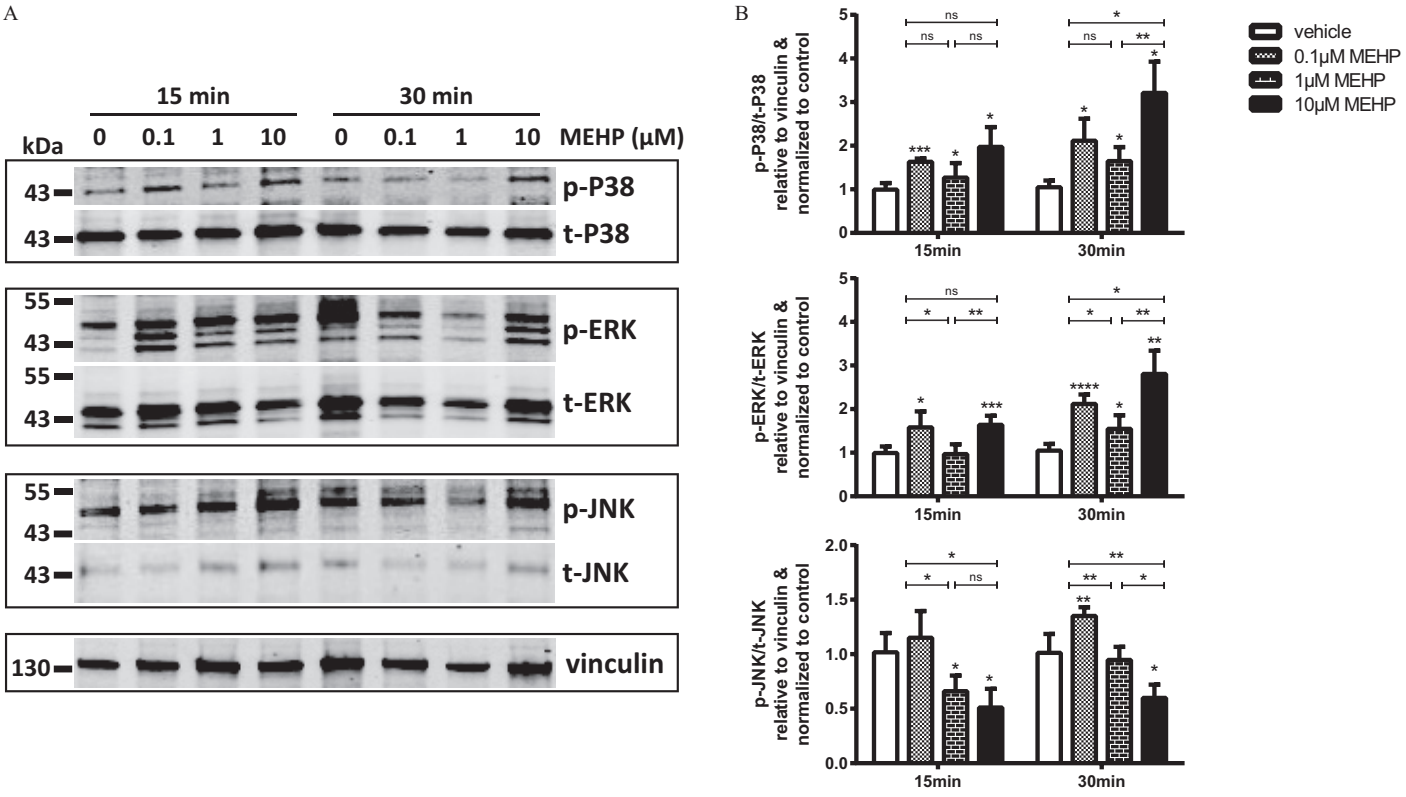

Figure 6. Effect of MEHP on the MAPK pathway. After 72 h of culture, *in vitro* differentiated VCTs were treated for 15 or 30 min with MEHP (0.1, 1, or 10 μM). (*A*) Representative images of western blots. Proteins (50 μg) were loaded in 4–12% Tris-Bis gradient gels, and then blots were probed with anti-p-ERK, t-ERK, p-P38, t-P38, p-JNK, t-JNK, and vinculin antibodies. (*B*) The protein level was calculated by densitometry using ImageJ. Values are presented as the mean + SD of the densitometric value relative to vinculin and normalized to vehicle control ($n = 3$). Note: DMSO, dimethylsulfoxide; MAPK, mitogen-activated protein kinases; MEHP, mono(2-ethylhexyl) phthalate; ST, syncytiotrophoblast. Statistical analysis was performed using paired *t*-tests in comparison with vehicle control; $*p < 0.05$, $**p < 0.01$, $***p < 0.001$, $****p < 0.0001$.

selectivity, at low vs. high doses (Vandenberg et al. 2012). In fact, several EDCs that have been shown to have low-dose effects are known to act via multiple receptors and pathways (Balaguer et al. 2017). Thus, the effects seen at high doses can be due to the binding of multiple receptors, whereas the effects of low doses may occur via only a single receptor or receptor family (Vandenberg et al. 2012). The mechanisms are likely to be complex, possibly with multiple targets and pathways affected in the same tissue or even different, tissue-specific responses from a single EDC (Vrooman et al. 2016). Additional experiments are required, such as co-treatment with a PPARγ antagonist and transcriptomic work to determine which receptors contribute to the MEHP responses observed in this study and whether PPARγ is the dominant receptor mediating MEHP's agonizing effects at a high dose.

To examine whether MEHP exposure affected lipid metabolism, we first examined lipid droplet accumulation using BODIPY labeling. We observed a concordance between the U-shaped pattern of PPARγ activation in MEHP-treated VCT and lipid droplet accumulation in MEHP-treated placental villi. It is interesting to note that these experiments showed that MEHP crossed the placental barrier and affected lipid contents in all cell types (ST, VCT, and MCs). Indeed, we observed greater accumulation of lipid droplets in mesenchymal cells after a 10 μM treatment with MEHP. As mesenchymal-trophoblast cross-talk has been proposed to play a major role in trophoblast cell fusion regulation (Pidoux et al. 2012), and as it has been described that adipogenic differentiation of mesenchymal stem cells is increased by secreted factors from adipose tissue (Wu et al. 2012), we can hypothesize that MCs (which could give rise to adipose cells) may secrete lipogenic factors that enhance PPARγ activation in VCT and ST though a paracrine process. Next, we conducted a global lipidomics analysis. Using OPLS-DA, we identified 115 lipids with differential expression in 10 μM MEHP-treated cells in comparison with control, and 50 lipids in 0.1 μM MEHP-treated cells, with only 20 lipids in common between the two treatments (Table S1). Our lipid profiling supports the idea that MEHP modifies lipid composition in a dose-dependent manner. It is interesting to note that cells treated with 10 μM MEHP showed significantly higher levels of two glycerophospholipids (PC, PS) than cells treated with the lower concentration did. Membranes of eukaryotic cells are composed principally of glycerophospholipids, mostly phosphatidylcholines (PC), which play a critical role in regulating the physical properties (called "fluidity") of the membrane. The concentrations of these lipids thus influence the function of membrane proteins and the movement of proteins within the membrane (Kanno et al. 2007), essential processes involved in cell fusion. Furthermore, 10 μM MEHP-treated cells showed significantly higher levels of numerous polyunsaturated fatty acids (FA; $n = 11/16$, Table S1) than 0.1 μM MEHP-treated cells did. These fatty acids are the principal precursors for the production of eicosanoids, such as prostaglandins, which are the natural ligands of PPARγ (Nosjean and Boutin 2002). It is also important to note that PPARγ activation can increase both esterification as well as lipolysis (Haemmerle et al. 2011; Zechner et al. 2012), which could explain the higher level of FA, MG, and DG in cells treated with 10 μM of MEHP. These results may suggest the existence of a positive feedback loop of MEHP on PPARγ activation and membrane fluidity that

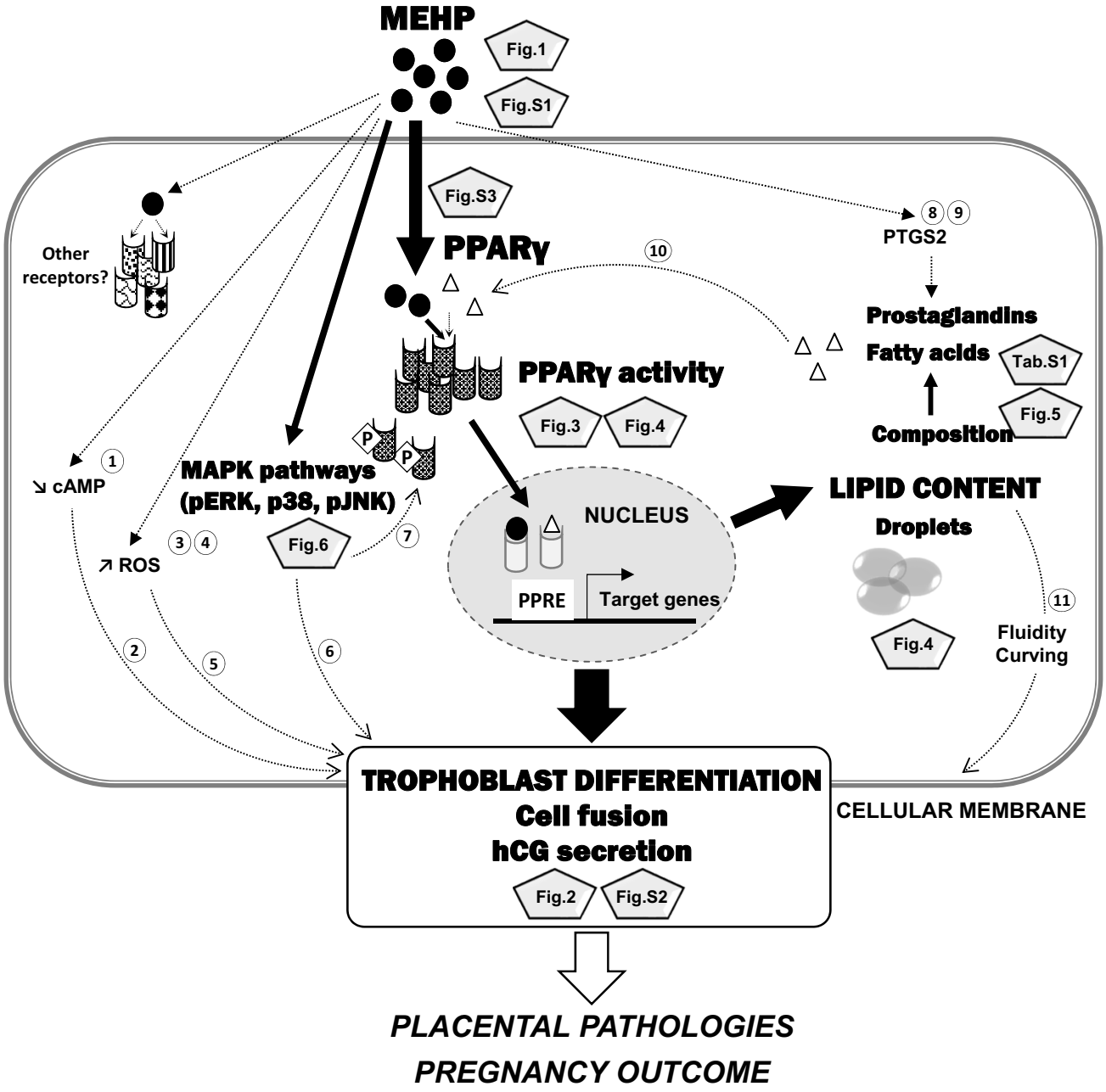

Figure 7. A proposed schematic diagram for MEHP impacts on villous cytotrophoblast cells. Features in solid black line and bold text represent results obtained in the present study; dashed lines represent potential regulation based on the literature (circle): [1](Lovekamp-Swan and Davis 2003), [2](Delidaki et al. 2011), [3](Meruvu et al. 2016), [4](Tetz et al. 2013), [5](Wu et al. 2015), [6](Vaillancourt et al. 2009), [7](Burns and Vanden Heuvel 2007), [8](Tetz et al. 2015), [9](Wang et al. 2016), [10](Marion-Letellier et al. 2016). Note: cAMP: Cyclic adenosine monophosphate; hCG, human chorionic gonadotropin; MAPK, mitogen-activated protein kinases; MEHP, mono(2-ethylhexyl) phthalate; PPARγ, peroxisome proliferator-activated receptor gamma; PPRE, peroxisome proliferator response element; PTGS2, prostaglandin-endoperoxide synthase 2; ROS, reactive oxygen species.

could explain the higher cell fusion observed in 10 μM MEHP-treated cells. In contrast, 0.1 μM MEHP-treated cells had significantly lower levels of all phosphatidic acid subclasses (PA, PA-P, LPA) than 10 μM MEHP-treated cells did. Phosphatidic acids have been shown to promote membrane fusion through their ability to change membrane topology called "curving" (Zeniou-Meyer et al. 2007). Therefore, the lack of PAs in 0.1 μM MEHP-treated cells could explain the low level of cell fusion observed.

As PPARγ has several sites of phosphorylation, PPARγ activity can be modulated by MAPKs, in particular ERKs; Burns and Vanden Heuvel 2007). Because MAPKs are involved in cytotrophoblast differentiation (Vaillancourt et al. 2009), and have been reported to be impaired in human trophoblast HTR-8/SVneo cells treated with an environmental EDC (Benzo(a)Pyrene; Liu et al. 2016), we further investigated the molecular mechanisms of MEHP by the MAPK pathways. The MAPKs comprise ERKs, P38, and JNK. We found that MEHP disturbed all of these pathways, but in a different manner. In the present study, we observed increased levels of p-ERK and p-P38, and a lower level of p-JNK in cells treated with 10 μM MEHP. This contrast could be explained by the fact that MAPKs are activated through distinct molecular signaling pathways. Activation of ERKs and P38 predominantly occurs through mitogenic stimuli, whereas the activation of JNK is mainly achieved through growth factors, environmental stresses, and proinflammatory stimuli (Kyriakis and Avruch 2012). To our knowledge, our findings are the first to elucidate the effects of MEHP on cytotrophoblast differentiation, specifically with respect to its influence on PPARγ and MAPK pathways. It is interesting to note that the transcriptional activity of PPARγ is affected by cross-talk with kinases and phosphatases. Phosphorylation by ERK and other kinases can affect its activity in either a ligand-dependent or ligand-independent manner. Indeed, the effects of phosphorylation depend on the cellular context, receptor subtype, and residue metabolized, which can manifest at several steps: ligand affinity (Rochette-Egly 2003; Shao et al. 1998), DNA binding (Rochette-Egly 2003; Shao et al. 1998), coactivator recruitment (Rochette-Egly 2003; Shao et al. 1998), and proteasomal degradation of PPARγ (Floyd and Stephens 2002).

Our study has a limitation. Given the origin of the placentas (Paris, France), the small size of samples, and the lack of demographic and biographical information for patients, our results may not be widely generalizable to other populations. However, even though it would be inadvisable to take our results completely at face value, the findings revealed here are largely consistent with previous studies and provide intriguing new avenues for study. In particular, our evidence of a U-shaped dose–response curve for MEHP clearly merits further investigation.

Conclusion

To conclude, this work suggested, to our knowledge for the first time, that MEHP has a U-shaped dose–response effect on PPARγ transcriptional activity as well as an impact on MAPK pathways, which together promote disturbances in lipid metabolism and in human VCT differentiation (Figure 7). Our results support a role for MEHP as an endocrine disruptor in human trophoblasts by inhibiting hCG secretion. To our knowledge, we are the first to report an impact of environmentally relevant concentrations of MEHP on human ST formation, which is essential for a fully functional placenta (Mayhew 2014). However, it is necessary to remember that organs are exposed to several phthalates that can accumulate and have additive or opposite effects, as recently described by Adibi et al. 2017b.

Acknowledgments

The authors wish to thank the consenting patients and the clinical staff midwives of Cochin Port-Royal, Antony, and Montsouris hospitals for providing placental tissues, the Cochin Institute and Université Paris Descartes Faculté de Pharmacie de Paris imaging facilities, and E. Guilloteau (Master of Science student) for preliminary results on the effect of MEHP on MAPK pathways. This work was supported by ANSES (PhthalatPreG project) and RSI professions libérales provinces, Paris, France.

References

Adibi JJ, Whyatt RM, Williams PL, Calafat AM, Camann D, Herrick R, et al. 2008. Characterization of phthalate exposure among pregnant women assessed by repeat air and urine samples. Environ Health Perspect 116(4):467–473, PMID: 18414628, https://doi.org/10.1289/ehp.10749.

Adibi JJ, Buckley JP, Lee MK, Williams PL, Just AC, Zhao Y, et al. 2017a. Maternal urinary phthalates and sex-specific placental mRNA levels in an urban birth cohort. Environ Health 16(1):35, PMID: 28381288, https://doi.org/10.1186/s12940-017-0241-5.

Adibi JJ, Zhao Y, Zhan LV, Kapidzic M, Larocque N, Koistinen H, et al. 2017b. An investigation of the single and combined phthalate metabolite effects on human chorionic gonadotropin expression in placental cells. Environ Health Perspect 125(10):107010, PMID: 29089286, https://doi.org/10.1289/EHP1539.

Alsat E, Mirlesse V, Fondacci C, Dodeur M, Evain-Brion D. 1991. Parathyroid hormone increases epidermal growth factor receptors in cultured human trophoblastic cells from early and term placenta. J Clin Endocrinol Metab 73(2):288–295, PMID: 1856260, https://doi.org/10.1210/jcem-73-2-288.

Aplin JD, Jones CJ. 2008. Human placental development. In: *The Endometrium: Molecular, Cellular and Clinical Perspectives*. Aplin JD F, A, Glasser SR, Giudice LJ, eds. 2nd ed. Boca Raton, FL: CRC Press.

Balaguer P, Delfosse V, Grimaldi M, Bourguet W. 2017. Structural and functional evidences for the interactions between nuclear hormone receptors and endocrine disruptors at low doses. C R Biol 340(9–10):414–420, PMID: 29126514, https://doi.org/10.1016/j.crvi.2017.08.002.

Barak Y, Nelson MC, Ong ES, Jones YZ, Ruiz-Lozano P, Chien KR, et al. 1999. PPAR gamma is required for placental, cardiac, and adipose tissue development. Mol Cell 4(4):585–595, PMID: 10549290, https://doi.org/10.1016/S1097-2765(00)80209-9.

Buck Louis GM, Sundaram R, Sweeney AM, Schisterman EF, Maisog J, Kannan K. 2014. Urinary bisphenol a, phthalates, and couple fecundity: the Longitudinal Investigation of Fertility and the Environment (LIFE) Study. Fertil Steril 101(5):1359–1366, PMID: 24534276, https://doi.org/10.1016/j.fertnstert.2014.01.022.

Burns KA, Vanden Heuvel JP. 2007. Modulation of PPAR activity via phosphorylation. Biochim Biophys Acta 1771(8):952–960, PMID: 17560826, https://doi.org/10.1016/j.bbalip.2007.04.018.

Chou K, Wright RO. 2006. Phthalates in food and medical devices. J Med Toxicol 2(3):126–135, PMID: 18077888, https://doi.org/10.1007/BF03161027.

Cocquebert M, Berndt S, Segond N, Guibourdenche J, Murthi P, Aldaz-Carroll L, et al. 2012. Comparative expression of hSG β-genes in human trophoblast from early and late first-trimester placentas. Am J Physiol Endocrinol Metab 303(8):E950–E958, PMID: 22811468, https://doi.org/10.1152/ajpendo.00087.2012.

Degrelle SA, Fournier T. 2018. Use of GATA3 and TWIST1 immunofluorescence staining to assess in vitro syncytial fusion index. Methods Mol Biol 1710:165–171, PMID: 29197002, https://doi.org/10.1007/978-1-4939-7498-6_13.

Degrelle SA, Gerbaud P, Leconte L, Ferreira F, Pidoux G. 2017a. Annexin-A5 organized in 2D-network at the plasmalemma eases human trophoblast fusion. Sci Rep 7:42173, PMID: 28176826, https://doi.org/10.1038/srep42173.

Degrelle SA, Shoaito H, Fournier T. 2017b. New transcriptional reporters to quantify and monitor PPARγ activity. PPAR Res 2017:6139107, PMID: 29225614, https://doi.org/10.1155/2017/6139107.

Delidaki M, Gu M, Hein A, Vatish M, Grammatopoulos DK. 2011. Interplay of cAMP and MAPK pathways in hCG secretion and fusogenic gene expression in a trophoblast cell line. Mol Cell Endocrinol 332(1–2):213–220, PMID: 21035520, https://doi.org/10.1016/j.mce.2010.10.013.

Engel SM, Zhu C, Berkowitz GS, Calafat AM, Silva MJ, Miodovnik A, et al. 2009. Prenatal phthalate exposure and performance on the neonatal behavioral assessment scale in a multiethnic birth cohort. Neurotoxicology 30(4):522–528, PMID: 19375452, https://doi.org/10.1016/j.neuro.2009.04.001.

Ferguson KK, McElrath TF, Meeker JD. 2014. Environmental phthalate exposure and preterm birth. JAMA Pediatr 168(1):61–67, PMID: 24247736, https://doi.org/10.1001/jamapediatrics.2013.3699.

Floyd ZE, Stephens JM. 2002. Interferon-gamma-mediated activation and ubiquitin-proteasome-dependent degradation of PPARgamma in adipocytes. J Biol Chem 277(6):4062–4068, PMID: 11733495, https://doi.org/10.1074/jbc.M108473200.

Fournier T, Guibourdenche J, Evain-Brion D. 2015. Review: hCGs: Different sources of production, different glycoforms and functions. Placenta 36 (Suppl 1):S60–S65, PMID: 25707740, https://doi.org/10.1016/j.placenta.2015.02.002.

Fournier T, Thérond P, Handschuh K, Tsatsaris V, Evain-Brion D. 2008. PPARgamma and early human placental development. Curr Med Chem 15(28):3011–3024, PMID: 19075649, https://doi.org/10.2174/092986708786848677.

Frendo JL, Cronier L, Bertin G, Guibourdenche J, Vidaud M, Evain-Brion D, et al. 2003. Involvement of connexin 43 in human trophoblast cell fusion and differentiation. J Cell Sci 116(Pt 16):3413–3421, PMID: 12840075, https://doi.org/10.1242/jcs.00648.

Gao F, Hu W, Li Y, Shen H, Hu J. 2017a. Mono-2-ethylhexyl phthalate inhibits human extravillous trophoblast invasion via the PPARγ pathway. Toxicol Appl Pharmacol 327:23–29, PMID: 28416457, https://doi.org/10.1016/j.taap.2017.04.014.

Gao H, Zhang YW, Huang K, Yan SQ, Mao LJ, Ge X, et al. 2017b. Urinary concentrations of phthalate metabolites in early pregnancy associated with clinical pregnancy loss in Chinese women. Sci Rep 7(1):6800, PMID: 28754983, https://doi.org/10.1038/s41598-017-06450-2.

Giannini S, Serio M, Galli A. 2004. Pleiotropic effects of thiazolidinediones: taking a look beyond antidiabetic activity. J Endocrinol Invest 27(10):982–991, PMID: 15762051, https://doi.org/10.1007/BF03347546.

Guibert E, Prieur B, Cariou R, Courant F, Antignac JP, Pain B, et al. 2013. Effects of mono-(2-ethylhexyl) phthalate (MEHP) on chicken germ cells cultured in vitro. Environ Sci Pollut Res Int 20(5):2771–2783, PMID: 23354615, https://doi.org/10.1007/s11356-013-1487-2.

Haemmerle G, Moustafa T, Woelkart G, Büttner S, Schmidt A, van de Weijer T, et al. 2011. ATGL-mediated fat catabolism regulates cardiac mitochondrial function via PPAR-α and PGC-1. Nat Med 17(9):1076–1085, PMID: 21857651, https://doi.org/10.1038/nm.2439.

Holdsworth-Carson SJ, Lim R, Mitton A, Whitehead C, Rice GE, Permezel M, et al. 2010. Peroxisome proliferator-activated receptors are altered in pathologies of the human placenta: gestational diabetes mellitus, intrauterine growth restriction and preeclampsia. Placenta 31(3):222–229, PMID: 20045185, https://doi.org/10.1016/j.placenta.2009.12.009.

Huang Y, Li J, Garcia JM, Lin H, Wang Y, Yan P, et al. 2014. Phthalate levels in cord blood are associated with preterm delivery and fetal growth parameters in Chinese women. PLoS One 9(2):e87430, PMID: 24503621, https://doi.org/10.1371/journal.pone.0087430.

Huppertz B, Gauster M. 2011. Trophoblast fusion. Adv Exp Med Biol 713:81–95, PMID: 21432015, https://doi.org/10.1007/978-94-007-0763-4_6.

Huppertz B, Kingdom JC. 2004. Apoptosis in the trophoblast–role of apoptosis in placental morphogenesis. J Soc Gynecol Investig 11(6):353–362, PMID: 15350247, https://doi.org/10.1016/j.jsgi.2004.06.002.

Jukic AM, Calafat AM, McConnaughey DR, Longnecker MP, Hoppin JA, Weinberg CR, et al. 2016. Urinary concentrations of phthalate metabolites and bisphenol A and associations with follicular-phase length, luteal-phase length, fecundability, and early pregnancy loss. Environ Health Perspect 124(3):321–328, PMID: 26161573, https://doi.org/10.1289/ehp.1408164.

Kambia N, Renault N, Dilly S, Farce A, Dine T, Gressier B, et al. 2008. Molecular modelling of phthalates - PPARs interactions. J Enzyme Inhib Med Chem 23(5):611–616, PMID: 18821250, https://doi.org/10.1080/14756360802205059.

Kanno K, Wu MK, Scapa EF, Roderick SL, Cohen DE. 2007. Structure and function of phosphatidylcholine transfer protein (PC-TP)/StarD2. Biochim Biophys Acta 1771(6):654–662, PMID: 17499021, https://doi.org/10.1016/j.bbalip.2007.04.003.

Kyriakis JM, Avruch J. 2012. Mammalian MAPK signal transduction pathways activated by stress and inflammation: a 10-year update. Physiol Rev 92(2):689–737, PMID: 22535895, https://doi.org/10.1152/physrev.00028.2011.

Latini G, De Felice C, Presta G, Del Vecchio A, Paris I, Ruggieri F, et al. 2003. In utero exposure to di-(2-ethylhexyl)phthalate and duration of human pregnancy. Environ Health Perspect 111(14):1783–1785, PMID: 14594632, https://doi.org/10.1289/ehp.6202.

Latruffe N, Vamecq J. 1997. Peroxisome proliferators and peroxisome proliferator activated receptors (PPARs) as regulators of lipid metabolism. Biochimie 79(2–3):81–94, PMID: 9209701.

Lin L, Zheng LX, Gu YP, Wang JY, Zhang YH, Song WM. 2008. [levels of environmental endocrine disruptors in umbilical cord blood and maternal blood of low-birth-weight infants]. Zhonghua Yu Fang Yi Xue Za Zhi [Chinese J Preventive Med] 42(3):177–180, PMID: 18788582.

Liu L, Wang Y, Shen C, He J, Liu X, Ding Y, et al. 2016. Benzo(a)pyrene inhibits migration and invasion of extravillous trophoblast HTR-8/SVneo cells via activation of the ERK and JNK pathway. J Appl Toxicol 36(7):946–955, PMID: 26359795, https://doi.org/10.1002/jat.3227.

Longtine MS, Chen B, Odibo AO, Zhong Y, Nelson DM. 2012. Villous trophoblast apoptosis is elevated and restricted to cytotrophoblasts in pregnancies complicated by preeclampsia, IUGR, or preeclampsia with IUGR. Placenta 33(5):352–359, PMID: 22341340, https://doi.org/10.1016/j.placenta.2012.01.017.

Lovekamp-Swan T, Davis BJ. 2003. Mechanisms of phthalate ester toxicity in the female reproductive system. Environ Health Perspect 111(2):139–145, PMID: 12573895, https://doi.org/10.1289/ehp.5658.

Lyche JL, Gutleb AC, Bergman A, Eriksen GS, Murk AJ, Ropstad E, et al. 2009. Reproductive and developmental toxicity of phthalates. J Toxicol Environ Health B Crit Rev 12(4):225–249, PMID: 20183522, https://doi.org/10.1080/10937400903094091.

Manteiga S, Lee K. 2017. Monoethylhexyl phthalate elicits an inflammatory response in adipocytes characterized by alterations in lipid and cytokine pathways. Environ Health Perspect 125(4):615–622, PMID: 27384973, https://doi.org/10.1289/EHP464.

Marion-Letellier R, Savoye G, Ghosh S. 2016. Fatty acids, eicosanoids and PPAR gamma. Eur J Pharmacol 785:44–49, PMID: 26632493, https://doi.org/10.1016/j.ejphar.2015.11.004.

Mayhew TM. 2014. Turnover of human villous trophoblast in normal pregnancy: what do we know and what do we need to know? Placenta 35(4):229–240, PMID: 24529666, https://doi.org/10.1016/j.placenta.2014.01.011.

McCarthy FP, Drewlo S, English FA, Kingdom J, Johns EJ, Kenny LC, et al. 2011. Evidence implicating peroxisome proliferator-activated receptor-γ in the pathogenesis of preeclampsia. Hypertension 58(5):882–887, PMID: 21931072, https://doi.org/10.1161/HYPERTENSIONAHA.111.179440.

Meruvu S, Zhang J, Choudhury M. 2016. Mono-(2-ethylhexyl) phthalate increases oxidative stress responsive miRNAs in first trimester placental cell line HTR8/SVneo. Chem Res Toxicol 29(3):430–435, PMID: 26871967, https://doi.org/10.1021/acs.chemrestox.6b00038.

Mose T, Mortensen GK, Hedegaard M, Knudsen LE. 2007. Phthalate monoesters in perfusate from a dual placenta perfusion system, the placenta tissue and umbilical cord blood. Reprod Toxicol 23(1):83–91, PMID: 17049806, https://doi.org/10.1016/j.reprotox.2006.08.006.

Nadra K, Quignodon L, Sardella C, Joye E, Mucciolo A, Chrast R, et al. 2010. PPARgamma in placental angiogenesis. Endocrinology 151(10):4969–4981, PMID: 20810566, https://doi.org/10.1210/en.2010-0131.

Nosjean O, Boutin JA. 2002. Natural ligands of PPARgamma: are prostaglandin J(2) derivatives really playing the part? Cell Signal 14(7):573–583, PMID: 11955950, https://doi.org/10.1016/S0898-6568(01)00281-9.

Pidoux G, Gerbaud P, Cocquebert M, Segond N, Badet J, Fournier T, et al. 2012. Review: human trophoblast fusion and differentiation: lessons from trisomy 21 placenta. Placenta 33 (Suppl):S81–S86, PMID: 22138060, https://doi.org/10.1016/j.placenta.2011.11.007.

Pidoux G, Gerbaud P, Guibourdenche J, Thérond P, Ferreira F, Simasotchi C, et al. 2015. Formaldehyde crosses the human placenta and affects human trophoblast differentiation and hormonal functions. PLoS One 10(7):e0133506, PMID: 26186596, https://doi.org/10.1371/journal.pone.0133506.

Pidoux G, Gerbaud P, Marpeau O, Guibourdenche J, Ferreira F, Badet J, et al. 2007. Human placental development is impaired by abnormal human chorionic gonadotropin signaling in trisomy 21 pregnancies. Endocrinology 148(11):5403–5413, PMID: 17690166, https://doi.org/10.1210/en.2007-0589.

Rochette-Egly C. 2003. Nuclear receptors: integration of multiple signalling pathways through phosphorylation. Cell Signal 15(4):355–366, PMID: 12618210, https://doi.org/10.1016/S0898-6568(02)00115-8.

Roland CS, Hu J, Ren CE, Chen H, Li J, Varvoutis MS, et al. 2016. Morphological changes of placental syncytium and their implications for the pathogenesis of preeclampsia. Cell Mol Life Sci 73(2):365–376, PMID: 26496726, https://doi.org/10.1007/s00018-015-2069-x.

Schaiff WT, Carlson MG, Smith SD, Levy R, Nelson DM, Sadovsky Y. 2000. Peroxisome proliferator-activated receptor-gamma modulates differentiation of human trophoblast in a ligand-specific manner. J Clin Endocrinol Metab 85(10):3874–3881, https://doi.org/10.1210/jcem.85.10.6885.

Schoonjans K, Staels B, Auwerx J. 1996. The peroxisome proliferator activated receptors (PPARs) and their effects on lipid metabolism and adipocyte differentiation. Biochim Biophys Acta 1302(2):93–109, PMID: 8695669, https://doi.org/10.1016/0005-2760(96)00066-5.

Segond N, Degrelle SA, Berndt S, Clouqueur E, Rouault C, Saubamea B, et al. 2013. Transcriptome analysis of PPARγ target genes reveals the involvement of lysyl oxidase in human placental cytotrophoblast invasion. PLoS One 8(11):e79413, PMID: 24265769, https://doi.org/10.1371/journal.pone.0079413.

Shao D, Rangwala SM, Bailey ST, Krakow SL, Reginato MJ, Lazar MA. 1998. Interdomain communication regulating ligand binding by PPAR-gamma. Nature 396(6709):377–380, PMID: 9845075, https://doi.org/10.1038/24634.

Song Q, Li R, Zhao Y, Zhu Q, Xia B, Chen S, et al. 2018. Evaluating effects of prenatal exposure to phthalates on neonatal birth weight: structural equation model approaches. Chemosphere 205:674–681, PMID: 29723725, https://doi.org/10.1016/j.chemosphere.2018.04.063.

Tarrade A, Schoonjans K, Guibourdenche J, Bidart JM, Vidaud M, Auwerx J, et al. 2001. PPAR gamma/RXR alpha heterodimers are involved in human CG beta

synthesis and human trophoblast differentiation. Endocrinology 142(10):4504–4514, PMID: 11564716, https://doi.org/10.1210/endo.142.10.8448.

Téllez-Rojo MM, Cantoral A, Cantonwine DE, Schnaas L, Peterson K, Hu H, et al. 2013. Prenatal urinary phthalate metabolites levels and neurodevelopment in children at two and three years of age. Sci Total Environ 461–462:386–390, PMID: 23747553, https://doi.org/10.1016/j.scitotenv.2013.05.021.

Tetz LM, Aronoff DM, Loch-Caruso R. 2015. Mono-ethylhexyl phthalate stimulates prostaglandin secretion in human placental macrophages and THP-1 cells. Reprod Biol Endocrinol 13:56, PMID: 26036283, https://doi.org/10.1186/s12958-015-0046-8.

Tetz LM, Cheng AA, Korte CS, Giese RW, Wang P, Harris C, et al. 2013. Mono-2-ethylhexyl phthalate induces oxidative stress responses in human placental cells in vitro. Toxicol Appl Pharmacol 268(1):47–54, PMID: 23360888, https://doi.org/10.1016/j.taap.2013.01.020.

Vaillancourt C, Lanoix D, Le Bellego F, Daoud G, Lafond J. 2009. Involvement of MAPK signalling in human villous trophoblast differentiation. Mini Rev Med Chem 9(8):962–973, PMID: 19601892, https://doi.org/10.2174/138955709788681663.

Vandenberg LN, Colborn T, Hayes TB, Heindel JJ, Jacobs DR Jr, Lee DH, et al. 2012. Hormones and endocrine-disrupting chemicals: low-dose effects and nonmonotonic dose responses. Endocr Rev 33(3):378–455, PMID: 22419778, https://doi.org/10.1210/er.2011-1050.

Vélez MP, Arbuckle TE, Fraser WD. 2015. Female exposure to phenols and phthalates and time to pregnancy: the Maternal-Infant Research on Environmental Chemicals (MIREC) Study. Fertil Steril 103(4):1011–1020, PMID: 25681860, https://doi.org/10.1016/j.fertnstert.2015.01.005.

Vrijheid M, Casas M, Gascon M, Valvi D, Nieuwenhuijsen M. 2016. Environmental pollutants and child health-a review of recent concerns. Int J Hyg Environ Health 219(4–5):331–342, PMID: 27216159, https://doi.org/10.1016/j.ijheh.2016.05.001.

Vrooman LA, Xin F, Bartolomei MS. 2016. Morphologic and molecular changes in the placenta: what we can learn from environmental exposures. Fertil Steril 106(4):930–940, PMID: 27523298, https://doi.org/10.1016/j.fertnstert.2016.08.016.

Waite LL, Louie RE, Taylor RN. 2005. Circulating activators of peroxisome proliferator-activated receptors are reduced in preeclamptic pregnancy. J Clin Endocrinol Metab 90(2):620–626, PMID: 15562025, https://doi.org/10.1210/jc.2004-0849.

Wang XK, Agarwal M, Parobchak N, Rosen A, Vetrano AM, Srinivasan A, et al. 2016. Mono-(2-ethylhexyl) phthalate promotes pro-labor gene expression in the human placenta. PLoS One 11(1):e0147013, PMID: 26751383, https://doi.org/10.1371/journal.pone.0147013.

Wu F, Tian FJ, Lin Y. 2015. Oxidative stress in placenta: health and diseases. Biomed Res Int 2015:293271, PMID: 26693479, https://doi.org/10.1155/2015/293271.

Wu L, Wang T, Ge Y, Cai X, Wang J, Lin Y. 2012. Secreted factors from adipose tissue increase adipogenic differentiation of mesenchymal stem cells. Cell Prolif 45(4):311–319, PMID: 22571453, https://doi.org/10.1111/j.1365-2184.2012.00823.x.

Xu Y, Cook TJ, Knipp GT. 2005. Effects of di-(2-ethylhexyl)-phthalate (DEHP) and its metabolites on fatty acid homeostasis regulating proteins in rat placental HRP-1 trophoblast cells. Toxicol Sci 84(2):287–300, PMID: 15647598, https://doi.org/10.1093/toxsci/kfi083.

Zechner R, Zimmermann R, Eichmann TO, Kohlwein SD, Haemmerle G, Lass A, et al. 2012. FAT SIGNALS–lipases and lipolysis in lipid metabolism and signaling. Cell Metab 15(3):279–291, PMID: 22405066, https://doi.org/10.1016/j.cmet.2011.12.018.

Zeniou-Meyer M, Zabari N, Ashery U, Chasserot-Golaz S, Haeberlé AM, Demais V, et al. 2007. Phospholipase D1 production of phosphatidic acid at the plasma membrane promotes exocytosis of large dense-core granules at a late stage. J Biol Chem 282(30):21746–21757, PMID: 17540765, https://doi.org/10.1074/jbc.M702968200.

Zhu YD, Gao H, Huang K, Zhang YW, Cai XX, Yao HY, et al. 2017. Prenatal phthalate exposure and placental size and shape at birth: a birth cohort study. Environ Res 160:239–246, PMID: 29028488, https://doi.org/10.1016/j.envres.2017.09.012.